# A demigration-based reflection full-waveform inversion workflow

*Ping Wang\*, Zhigang Zhang, Zhiyuan Wei, and Rongxin Huang (CGG)*

## Summary

Reflection FWI is effective at providing low-wavenumber velocity updates for deep areas beyond the penetration depth of diving waves and significantly improves seismic imaging. However, the tomographic term of the FWI gradient that is good for low-wavenumber velocity updates can be contaminated by the stronger high-wavenumber migration term. We present a reflection FWI workflow that is based on Born modeling to explicitly generate the tomographic term and thus is minimally impacted by migration contamination. In addition, we propose to use a set of partial stacks as reflectivity models for Born modeling to reduce the risks of cycle-skipping and incorrect update sign and to use a traveltime cost function to mitigate the negative impact from amplitude mismatch between input data and modeled synthetic data. Finally, we demonstrate the benefit and effectiveness of our approach using a field data set from the Gulf of Mexico.

## Introduction

Conventional full-waveform inversion (FWI) (Tarantola, 1984) has become a standard for high-resolution velocity updates on top of ray-based reflection tomography. However, it is mostly driven by diving waves (Sirgue and Pratt, 2004) and usually can only resolve the velocity for the shallow region due to the limited depth of penetration. To resolve the velocity for deep targets, reflection energy is needed for the inversion. Mora (1989) demonstrated that such energy generates FWI gradients of two types: the tomographic term and the migration term. The main issue is that the migration term has almost no impact on the kinematics but is much stronger than the tomographic term because the former corresponds to first-order scattering, one order lower than the latter. Therefore, it is important to suppress the migration term for low-wavenumber velocity updates.

Similar to the reflection FWI (RFWI) workflow presented by Irabor and Warner (2016), Gomes and Chazalnoel (2017) propose a two-stage strategy to mitigate the negative impact of the migration term. In the first stage, an artificial density model is derived from the migration term. This density model contains the sharp contrasts needed to produce the tomographic term for the low-wavenumber velocity update in the second stage. Wavefield decomposition based on the vertical Hilbert transform is used to separate the migration term and the tomographic term (Liu et al., 2011; Tang et al., 2013). This workflow proves to be very effective in improving the velocity and the seismic image for deep targets (Jonke et al., 2017). However, strong migration leakage may be observed

around high-dip events due to the limitation of the vertical Hilbert transform.

One approach to naturally avoid the negative impact of the migration term is to decompose the velocity model (Xu et al., 2012; Sun et al., 2016). In this approach, the model is first decomposed into long-wavenumber and short-wavenumber components. Next, Born modeling (or so called "demigration") is performed using the former as the background velocity model and the latter as the reflectivity model to explicitly generate the low-wavenumber tomographic term (the so-called "rabbit ears"). One benefit of demigration using the migrated stack image as a reflectivity model is that the kinematics of the synthetic data are often close to that of the input data at near offsets. However, when the velocity error is large, cycle-skipping may still happen at large offsets as their imaging points can be far away from the stationary stacking points. This can lead to an RFWI gradient with wrong directions for long-offset data. In addition, like most other FWI approaches, the amplitude mismatch between input data and modeled synthetic data causes difficulties in computing the data residual and velocity gradient.

We present an RFWI workflow that adopts Born modeling to explicitly generate the tomographic term, uses a set of partial stacks as reflectivity models to mitigate the possibility of cycle-skipping and wrong update sign issues, and uses a traveltime cost function to partly address the amplitude mismatch between input data and modeled synthetic data. We illustrate the benefit and effectiveness of our approach with synthetic data as well as a field data set from the Gulf of Mexico (GoM).

## Method

Conventional FWI seeks a model $m(x)$ that minimizes the square residual cost function:

$$C(m) = \iiint ds\, dr d\omega \frac{1}{2}\|R(r, \omega, s; m)\|^2 \ , \qquad (1)$$

where $R(r, \omega, s; m)$ is the data residual between input data $d_0(r, \omega, s)$ and modeled synthetic data $d_{syn}(r, \omega, s; m)$, with $s$ and $r$ as the source and receiver locations and $\omega$ as the angular frequency. This equation is normally solved with gradient-based methods, and the gradient can be written as:

$$g(x) = \iint ds dr \int \omega^2 S(x, \omega, s; m) R(r, \omega, x; m) d\omega \ , \ (2)$$

with $S(x, \omega, s; m)$ as the source wavefield and $R(s, \omega, x; m)$ as the back-propagated residual wavefield at location $x$. Supposing we can decompose the input data and synthetic data into diving waves and reflection waves, the FWI gradient computed using Equation 2 with reflection energy as input data contains two terms: the migration term

**Demigration RFWI**

and the tomographic term (Mora, 1989; Figure 1a). In the rest of this section, we first compare two existing approaches for extracting the tomographic term from the RFWI gradient (Gomes and Chazalnoel, 2017; Xu et al., 2012) and then introduce our new RFWI strategy, which is free from migration leakage and better handles cycle-skipping and amplitude mismatch between input data and synthetic data.

1. RFWI based on wavefield decomposition

The gradient in Equation 2 can be separated into two terms using the wavefield decomposition method proposed by Liu et al. (2011):

$$\begin{cases} g_t(x) = \frac{1}{2} \iint ds dr \int \omega^2 [S(x,\omega,s)R(r,\omega,x;m) \\ \qquad + H_z(S(x,\omega,s))H_z(R(r,\omega,x;m))]d\omega \\ g_m(x) = \frac{1}{2} \iint ds dr \int \omega^2 [S(x,\omega,s)R(r,\omega,x;m) \\ \qquad - H_z(S(x,\omega,s))H_z(R(r,\omega,x;m))]d\omega \end{cases}, \quad (3)$$

where $H_z$ represents the Hilbert transform in the vertical direction, and $g_t(x)$ and $g_m(x)$ are the tomographic and migration terms, respectively. This equation sets up the key to the two-stage RFWI scheme proposed by Gomes and Chazalnoel (2017): 1) in the first stage, the high-wavenumber component $g_m(x)$ of the gradient is used to estimate an artificial density model serving as the sharp contrast for rabbit ear generation; 2) in the second stage,

the low-wavenumber component $g_t(x)$ of the gradient is used to update the velocity model. This decomposition-based RFWI is effective overall at extracting the tomographic term for the low-wavenumber velocity update, but with some contamination around high-dip structures from the migration term due to the intrinsic limitation of the vertical Hilbert transform (Figure 1b).

2. RFWI based on Born modeling

Instead of using wavefield decomposition to separate the migration and tomographic terms, this approach first splits the velocity model into two parts (Xu et al., 2012):

$$m = m_0 + \delta m, \quad (4)$$

where $m_0$ contains the long-wavelength components and $\delta m$ contains the short-wavelength components. It then also uses a two-step procedure: 1) in the first step, the background model $m_0$ is fixed to update $\delta m$, similar to least-squares migration (with the gradient being the same as that in Equation 2 but requiring a Laplacian filter or other filters to remove the backscattered noise); 2) in the second step, the short-wavelength model $\delta m$ is fixed to update $m_0$, where the rabbit ears are explicitly computed using $\delta m$ as the reflectivity model and the current background velocity model $m_0$:

$$g_d(x) = \iiint \omega^2 [\tilde{S}(x,\omega,s;m_0,\delta m)R(r,\omega,x;m_0) \\ + S(x,\omega,s;m_0)\tilde{R}(r,\omega,x;m_0,\delta m)]d\omega ds dr, \quad (5)$$
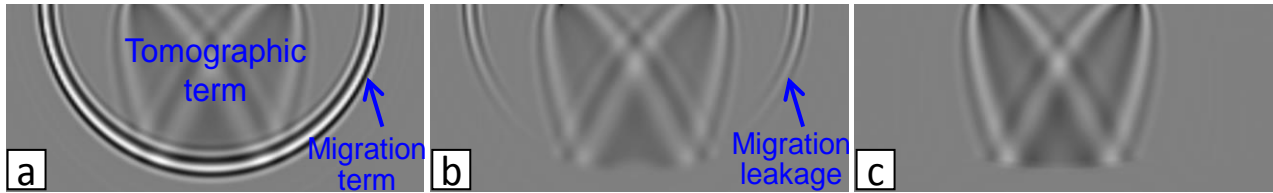


**Figure 1:** Gradient for one single trace and one single reflection event: a) conventional FWI; b) decomposition-based RFWI; c) demigration-based RFWI. The migration term leakage in b) is due to the limitation of wavefield decomposition using the vertical Hilbert transform.
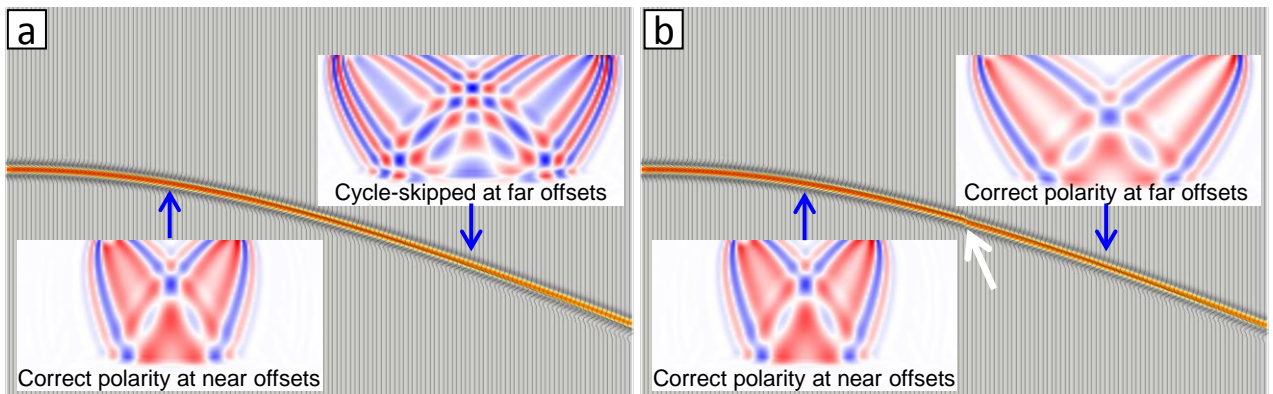


**Figure 2:** Shot-domain data and gradient for sample traces at near and far offsets produced when a) one and b) two offset classes are used for reflectivity models during Born modeling to generate synthetic data (red/orange event), wiggle input data. Note that there is a timing change (marked by white arrow) of the synthetic data in the middle of the shot gather in b) that effectively reduces the timing difference between input data and synthetic data at large offsets.

where $\tilde{S}$ and $\tilde{R}$ are the first-order source and receiver scattered wavefields (generated through Born modeling), respectively. The benefit of this approach is that it is free from migration contamination if the velocity background is smooth (Figure 1c) because only the second-order scattering is kept in the gradient through the crosscorrelation between the source or receiver (residual) wavefield and the first-order scattered energy from Born modeling. Hereinafter, we call methods of this class demigration-based RFWI. There are two major challenges: the first is the amplitude mismatch between input data and modeled synthetic data during residual computation ($R$ and $\tilde{R}$ in Equation 5), which is common to most FWI approaches; the second one, which is unique to RFWI, is that it uses a stack image as the reflectivity/density model for scattered wavefield computation. Next, we elaborate on these two challenges and describe how our proposed RFWI flow handles them.

3. An upgraded demigration-based RFWI workflow

Acoustic Born-modeled synthetic data often have different amplitudes compared to the recorded input data. This requires some sort of data matching when computing the data residual, which is often very challenging especially at the very low-frequency end due to amplitude-tuning among different events and contamination from strong noise. To partly mitigate this problem, we can use crosscorrelation-type cost functions (Choi and Alkhalifah, 2011; Xu et al., 2012) or traveltime cost functions that minimize the time shifts between input and modeled synthetic data (Luo and Schuster, 1991; Chi et al., 2015).

Errors in the velocity model introduce inaccuracy to the location of reflectors in the reflectivity model (migration image). Assuming the true velocity is overall slow and thus the event is curving-down on the common image point gather, and if the depth of the event on the stack image is driven by near offsets, it may be modeled earlier than the true data at far offsets. Conversely, if the location of the event is mostly driven by far offsets, it can arrive later than the true data at near offsets. When velocity errors are small and thus no cycle-skipping issue exists, the former may give a gradient with the correct sign while the latter gives a gradient with an opposite (wrong) sign. Moreover, when velocity errors are large, the cycle-skipping issue may further complicate the situation. To mitigate the chance of an incorrect update sign, as well as the risk of cycle-skipping, we propose to split the input data into offset classes and then generate reflectivity models using only the input data at smaller offsets from each class.

Figure 2 shows a simple 1D velocity and one reflector case where the reflector location in the reflectivity model is determined by near offset data, which happens most of the time in the real world. Therefore, the synthetic data generated using the reflectivity model have timing

consistent with near offsets and thus the gradient polarity is correct at near offsets (Figure 2a). However, because the velocity here is too slow, the timing difference between input data and synthetic data is large at far offsets and therefore the gradient has the opposite sign with oscillatory patterns at far offsets due to cycle-skipping. In Figure 2b, the cycle-skipping issue observed in the right inset of Figure 2a is corrected after we split the data into two offset classes.

**Field data examples**

We applied our RFWI scheme to a full-azimuth data set from the GoM. The initial velocity model was obtained after several iterations of ray-based reflection tomography and diving-wave FWI for the overburden, followed by salt interpretation and subsalt velocity updates. Data pre-processing steps for RFWI included denoise, source and receiver deghosting, designature, surface-related multiple elimination, and shot-domain data regularization. The diving-wave penetration depth for this data set is about 6 km for a maximum offset of 18 km along the cable. In addition, the gather quality in the deep area is very poor for ray-based reflection tomography. Therefore, RFWI is required for deep targets at depths ranging from 6 to 10 km.

With Figure 3, we demonstrate the benefit of demigration-based RFWI over decomposition-based RFWI in terms of migration term leakage. Figures 3a and 3b show the velocity perturbation overlaid on the raw RTM stack after decomposition-based and demigration-based RFWI, respectively. Migration leakage was observed around the salt boundary, especially the salt flank, in Figure 3a because those events involved strong energy with large wave-propagation angles in the source and receiver wavefields. On the contrary, the velocity perturbation obtained using demigration-based RFWI (3b) was free from such leakage. The zoomed-in sections in Figures 3c-e show that, while decomposition-based RFWI (3d) slightly improved the subsalt image, demigration-based RFWI (3e) performed better in that particular area.

Figure 4b shows the inline and crossline sections after our demigration-based RFWI. Compared to those from the initial model, the RFWI results have much better focusing and event continuity in the subsalt area, though there remains room for further improvement.

**Discussion and conclusions**

We have presented an RFWI workflow that adopts Born modeling to explicitly generate the tomographic term, and thus is minimally impacted by migration contamination. Furthermore, it uses a set of partial stacks as reflectivity models for Born modeling to reduce the possibility of cycle-skipping as well as incorrect update sign issues. In addition, it uses a traveltime cost function to mitigate the negative impact from amplitude mismatch between input

data and modeled synthetic data. We demonstrated with a field data example that our approach can help improve the image for deep targets where diving-wave FWI and ray-based reflection tomography are insufficient.

We noticed that the velocity update from our demigration-based RFWI has low resolution, especially in the vertical direction, because 1) the update is driven by reflection data with the transmission image condition and thus is intrinsically in low wavenumbers; 2) the update is mostly dominated by a few strong events; and 3) the angle range of the deep reflection data is limited. A scheme that improves the resolution by better addressing these limitations should further improve RFWI results.
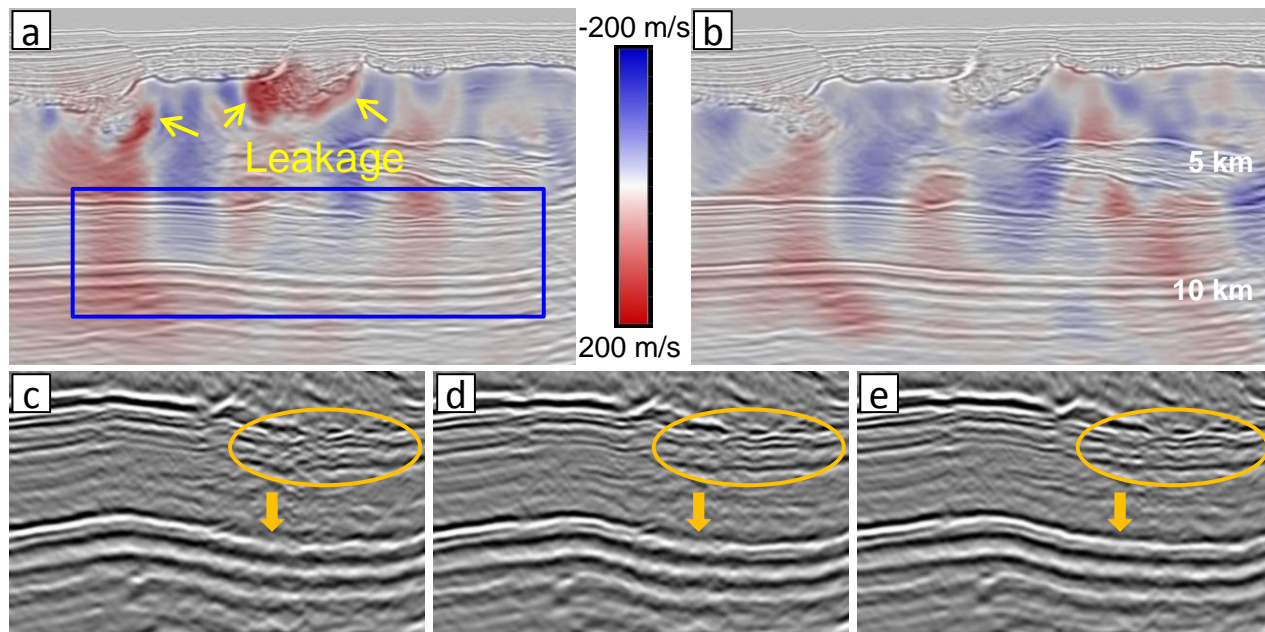
### Acknowledgments

**Figure 3:** Inline section with the velocity perturbation overlaid on RTM stack for: a) decomposition-based RFWI updated model and b) demigration-based RFWI updated model. Zoomed-in section for RTM stack in the blue box for: c) initial model, d) decomposition-based RFWI updated model, and e) demigration-based RFWI updated model.
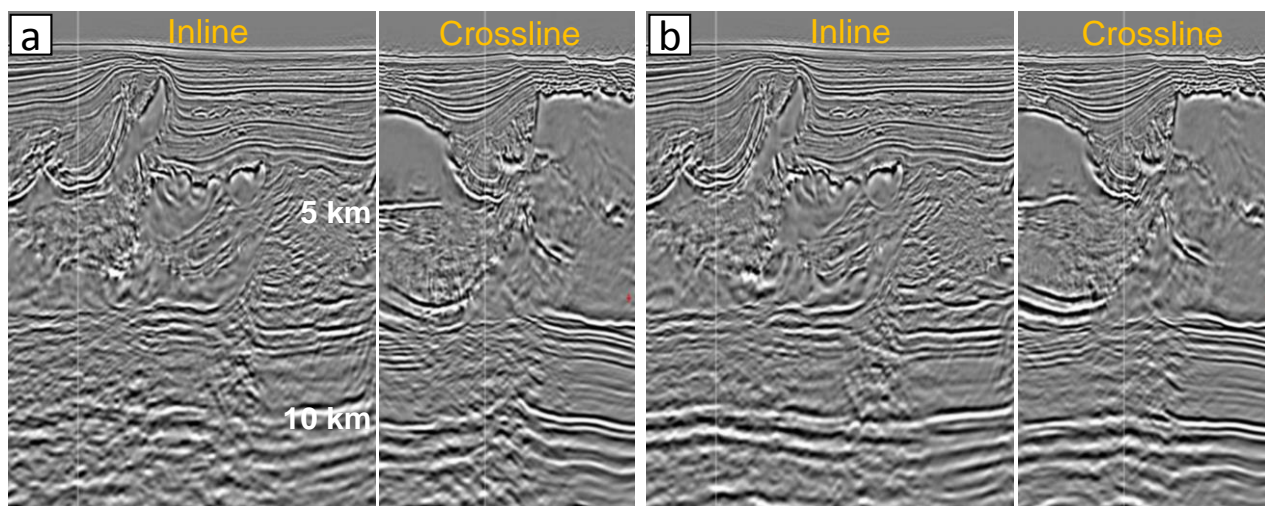


**Figure 4:** Inline and crossline sections of RTM stack for: a) initial model and b) demigration-based RFWI updated model.

# REFERENCES

Choi, Y., and T. Alkhalifah, 2011, Source-independent time-domain waveform inversion using convolved wavefields application to the encoded multisource waveform inversion: Geophysics, **76**, no. 5, R125–R134, https://doi.org/10.1190/geo2010-0210.1.

Chi, B., L. Dong, and Y. Liu, 2015, Correlation-based reflection full-waveform inversion: Geophysics, **80**, no. 4, R189–R202, https://doi.org/10.1190/geo2014-0345.1.

Gomes, A., and N. Chazalnoel, 2017, Extending the reach of FWI with reflection data: Potential and challenges: 87th Annual International Meeting, SEG, Expanded Abstracts, 1454–1459, https://doi.org/10.1190/segam2017-17731403.1.

Irabor, K., and M. Warner, 2016, Reflection FWI: 86th Annual International Meeting, SEG, Expanded Abstracts, 1136–1140, https://doi.org/10.1190/segam2016-13944219.1.

Jonke, K., Z. Fu, B. Wray, and H. Shen, 2017, Improving mini-basin and subsalt imaging with reflection full waveform inversion: 87th Annual International Meeting, SEG, Expanded Abstracts, 1492–1496, https://doi.org/10.1190/segam2017-17661070.1.

Liu, F., G. Zhang, S. Morton, and J. Leveille, 2011, An effective imaging condition for reverse-time migration using wavefield decomposition: Geophysics, **76**, no. 1, S29–S39, https://doi.org/10.1190/1.3533914.

Luo, Y., and G. T. Schuster, 1991, Wave-equation traveltime inversion: Geophysics, **56**, 645–653, https://doi.org/10.1190/1.1443081.

Mora, P., 1989, Inversion = migration + tomography: Geophysics, **54**, 1575–1586, https://doi.org/10.1190/1.1442625.

Sirgue, L., and G. Pratt, 2004, Efficient waveform inversion and imaging: A strategy for selecting temporal frequencies: Geophysics, **69**, 231–248, https://doi.org/10.1190/1.1649391.

Sun, D., K. Jiao, X. Cheng, and D. Vigh, 2016, Reflection based waveform inversion: 86th Annual International Meeting, SEG, Expanded Abstracts, 1151–1156, https://doi.org/10.1190/segam2016-13966097.1.

Tang, Y., S. Lee, A. Baumstein, and D. Hinkley, 2013, Tomographically enhanced full wavefield inversion: 83rd Annual International Meeting, SEG, Expanded Abstracts, 1037–1041, https://doi.org/10.1190/segam2013-1145.1.

Tarantola, A., 1984, Inversion of seismic reflection data in the acoustic approximation: Geophysics, **49**, 1259–1266, https://doi.org/10.1190/1.1441754.

Xu, S., D. Wang, F. Chen, Y. Zhang, and G. Lambaré, 2012, Full waveform inversion for reflected seismic data: 74th Annual International Conference and Exhibition, EAGE, Extended Abstracts, W024, https://doi.org/10.3997/2214-4609.20148725.